# Investigating the Thermodynamics of Radiative Cooling Materials through Simulations and Experiments

Senior thesis

Submitted by

Max R. Rudin

Advisor: Dr. Henry Everitt

Department of Physics and Astronomy
Rice University
Houston. April 2025

RICE UNIVERSITY

# Acknowledgements

I would like to thank my advisor, Dr. Henry Everitt, for guiding me through my research and helping me overcome hurdles in data analysis and experimental design. I would like to thank our colleague Dr. Mark Griep, and his team at the DEVCOM Army Research Laboratory (ARL) in Aberdeen, Maryland, for manufacturing the samples I tested and providing me with their Fourier-transform infrared spectroscopy (FTIR) absorbance data. I appreciate the training by Dr. Christopher Kuhs on how to run indoor and outdoor radiative cooling experiments and by Dr. Keith Sanders on creating steady-state Python simulations of heat transfer. I thank them both for their assistance.

# Contents

# Abstract

I studied the potential for radiative cooling materials to be used in rooftop air conditioning applications. I tested five experimental samples consisting of microscopic silica ($SiO_2$) beads suspended in styrene-ethylene-butylene-styrene (SEBS) polymer layers. I compared them to an identical SEBS control sample without any beads inside it. The microscopic beads are highly emissive in the infrared atmospheric transparency window (the 8 to 13 $\mu$m range of wavelengths), while the polymer is not, so I expected the experimental samples to outperform the control sample. Instead, I found that cooling is highly dependent on weather conditions, although the exact relationship between weather and cooling remains uncertain. Comparing the control sample to a bare aluminum plate, I found that the control sample itself (and therefore the SEBS polymer alone) has significant radiative cooling properties that should be investigated further.

# Chapter 1

# An Engineering Problem with a Physics Solution

## 1.1 Air Conditioning and Electricity Consumption

Air conditioning represents a significant portion of the electricity expenditure of homes and commercial buildings in the United States—about 9% each, as can be seen in Figure 1.1. This electricity costs consumers money while releasing carbon dioxide into the atmosphere. A method to cool buildings without the use of electricity would cut back on consumer costs and emissions. One method for electricity-free cooling relies on the physics of radiative heat transfer. This method, called "radiative cooling," would see rooftops coated with materials that are designed to cool down by emitting a lot of infrared light. If cost-effective, implementing these materials in construction could represent a benefit for consumers seeking to reduce costs and policy-makers seeking to reduce carbon emissions. Fundamental research on radiative cooling materials has been conducted in highly controlled environments, such as vacuum chambers [1], but radiative cooling in practical environments is still in its early stages of research.

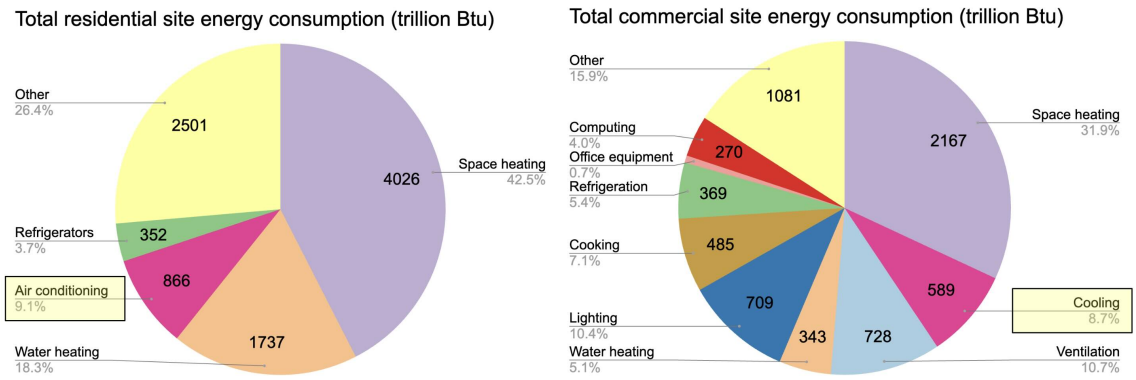


Figure 1.1: The most recent data from the U.S. Energy Information Administration on electricity consumption by end use [2], [3]. The air conditioning category for residential buildings and the cooling category for commercial buildings represent the electricity consumed for the purpose of cooling these types of buildings in the United States.

## 1.2 The Physics of Radiative Cooling

All matter is constantly emitting electromagnetic radiation, and through this emission, transferring heat into its environment. The amount of radiation, and the wavelengths at which it is emitted, are largely determined by the temperature of the emitter. This is Planck's law, and it defines the blackbody radiation spectrum, which is the amount of power per unit surface area a perfect emitter outputs at each wavelength of light. This spectrum is defined by Equation 1.1, which relates a given wavelength of light, $\lambda$, to the blackbody spectral intensity, $B_\lambda$, at that wavelength.

$$B_\lambda(\lambda, T) = \frac{2hc^2}{\lambda^5} \frac{1}{e^{\frac{hc}{\lambda k_B T}} - 1} \tag{1.1}$$

A material's properties impact its true emission spectrum. These impacts are described by a material's emissivity, $\epsilon(\lambda)$, which is a spectrum of unitless values between 0 and 1 that represents how much light a material actually emits relative to the blackbody spectrum. One can find a material's true spectral intensity by

multiplying the blackbody spectrum by the emissivity, as shown in Equation 1.2.

$$I_{\text{rad},\lambda}(\lambda) = B_\lambda(\lambda, T) \cdot \epsilon(\lambda) \tag{1.2}$$

To derive the total radiative power of a material per unit surface area (its total intensity), one must integrate this spectral intensity over the electromagnetic spectrum, as demonstrated in Equation 1.3.

$$I_{\text{rad}} = \int_0^\infty I_{\text{rad},\lambda}(\lambda)\, d\lambda \tag{1.3}$$

This calculation finds the total radiative power per unit surface area of a given material at a given temperature, and that is equivalent to the rate of heat transfer per unit area due to radiative cooling out of the material.

However, matter is also constantly absorbing electromagnetic radiation from its environment, and through this absorption, receiving heat from its environment. Depending on the material, a different proportion of the radiation that strikes a surface is absorbed by it (the rest is either reflected, scattered, or transmitted). This proportion is determined by a material's absorptivity, which is a spectrum of unitless values between 0 and 1 that describes what proportion of incident light of a given wavelength is actually absorbed. For a material to cool down via thermal radiation, it must emit more light than it absorbs (i.e. release more heat than it receives). However, because of Kirchhoff's law of thermal radiation, the emissivity and absorptivity spectra of a material must be precisely equal, making it difficult for a material to emit more without also absorbing more.

Thus, to accomplish radiative cooling, a material must be engineered to maximize emissivity in the wavelengths it emits most and minimize emissivity in the wavelengths it absorbs most. This means maximizing emissivity in the wavelength range around the peak of the blackbody spectrum at the operational temperature of the radiative cooling device. It means maximizing emissivity in ranges where any medium surrounding the device (in this case, air) is transparent (else the heat might be reabsorbed by nearby fluid, creating a heated pocket around the device that diminishes cooling). It also means minimizing emissivity, and thus absorptivity, in any range where the device is receiving a lot of light from its environment. For daytime

radiative cooling applications on rooftops, this means maximizing emissivity in the infrared atmospheric transparency window (the 8 to 13 $\mu$m range of wavelengths) and minimizing it in the peak solar radiation range (between 0.2 and 4 $\mu$m).

The infrared atmospheric transparency window from wavelengths of 8 to 13 $\mu$m represents both the peak of blackbody radiation at 300 K and a range in which the atmosphere is transparent. The peak emission wavelength of a blackbody can be found by taking the derivative of Planck's law (Equation 1.1) and setting it equal to zero. Performing this derivation, one finds that the peak emission wavelength of a blackbody is inversely proportional to its temperature (multiplied by a proportionality constant, $b$), a result known as Wien's displacement law. According to this law, blackbody radiation at 300 K has a peak near 10 $\mu$m, as calculated in Equation 1.4.

$$\lambda_{\text{peak}} = \frac{b}{T} = \frac{2.898 \times 10^{-3}\text{m} \cdot \text{K}}{300\text{K}} = 9.66 \times 10^{-6}\text{m} = 9.66\mu\text{m} \tag{1.4}$$

Therefore, maximizing emissivity around 10 $\mu$m has the most potential to increase radiative cooling. Furthermore, the 8 to 13 $\mu$m range also covers the atmosphere's infrared transparency window. The atmosphere is transparent in this range, meaning that radiated light can propagate freely through it. This allows radiated heat to efficiently travel away from the radiative cooling device and out into space. Also, it means that the atmosphere itself emits very little light in this range, which is important, because a high-emissivity material will absorb a lot of the light emitted by its environment. Thus, maximizing emissivity in the infrared atmospheric transparency window is critical when optimizing a material for radiative cooling.

The peak solar radiation range from 0.2 to 4 $\mu$m represents the majority of the light that will strike the radiative cooling device. This can also be demonstrated with Wien's displacement law by approximating the sun as a blackbody with a temperature of 6000 K. This calculation predicts that the sun has its radiation peak near 0.5 $\mu$m, as can be seen in Equation 1.5.

$$\lambda_{\text{peak}} = \frac{b}{T} = \frac{2.898 \times 10^{-3}\text{m} \cdot \text{K}}{6000\text{K}} = 4.83 \times 10^{-7}\text{m} = 0.483\mu\text{m} \tag{1.5}$$

This approximation is confirmed by the exact data for the solar intensity spectrum

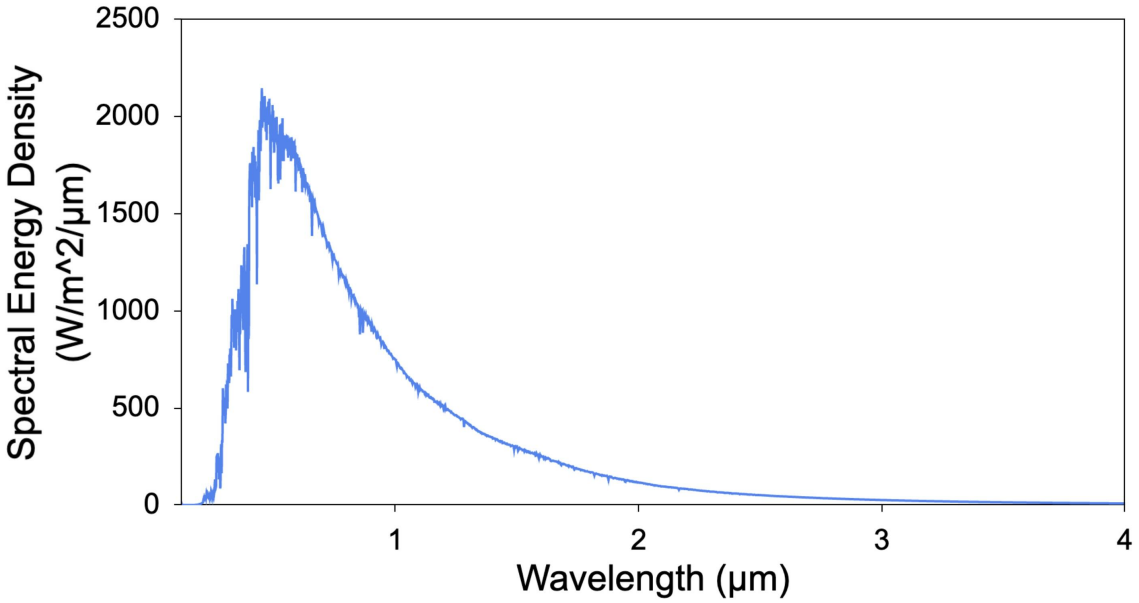


Figure 1.2: A graph of the spectral intensity of solar radiation received by the Earth's surface [4]. These data are used in my daytime Python simulations in chapter 2 to determine the impact of solar heating on radiative cooling materials.

displayed in Figure 1.2. Thus, minimizing emissivity in the 0.2 to 4 $\mu$m range is also critical for radiative cooling.

The question that remains is the relative importance of these two wavelength ranges to radiative cooling. My first round of Python simulations (discussed further in section 2.2) demonstrated that minimizing emissivity in the peak solar radiation range is more impactful than maximizing it in the infrared atmospheric transparency window.

## 1.3 Experimental Materials and Samples

The samples I experimented with consisted of silica ($SiO_2$) beads suspended in styrene-ethylene-butylene-styrene (SEBS) polymer layers. Each experimental sample contained a different-sized bead, including beads with diameters of 0.5 $\mu$m, 1 $\mu$m, 2 $\mu$m, 4 $\mu$m, and 8 $\mu$m. The control sample was a SEBS layer without any silica in it.

The absorbance spectra of these samples were measured using Fourier-transform infrared spectroscopy (FTIR), a method to measure the absorbance and transmission spectra of materials by measuring the amplitudes of infrared beams before and after interacting with a sample. These measurements were collected by Dr. Griep's team at the DEVCOM Army Research Laboratory (ARL) in Aberdeen, Maryland. The measurements were taken in attenuated total reflection (ATR) mode (where the infrared beam is reflected off the sample) because the samples were too thick and attenuated too much light in transmission mode (where the infrared beam passes through the sample). I converted the absorbance spectra that these measurements produced into transmission spectra via Equation 1.6.

$$T = 10^{-a} \tag{1.6}$$

When light interacts with matter it can either be transmitted, absorbed, reflected, or scattered. Therefore, the corresponding coefficients for these quantities (transmittance ($T$), absorptance ($A$), reflectance ($R$), and the scattering coefficient ($S$)) must sum to 1. This means that the absorbance data collected by ARL can be used to find an upper bound on absorptance, and since absorptance equals emissivity by Kirchhoff's law, this limit is also an upper bound on the emissivity, as shown in Equation 1.7.

$$1 - 10^{-a} = 1 - T = A + R + S \geq A = \epsilon \tag{1.7}$$

Since I am unsure about the degree of reflection and scattering in the samples, an upper bound on emissivity is all that can be gleamed from the data for now. However, future research into the reflection and scattering coefficients could prove fruitful in explaining some of the behaviors of the samples I observed in my experiments in chapter 3.

I plotted this upper bound of the samples' emissivities in Figure 1.3. The most important difference between the experimental and control sample emissivity spectra is the presence or lack of a peak in the infrared atmospheric transparency window. While the experimental samples (particularly those with smaller bead diameters) have a peak, the control sample does not. Since maximizing emissivity between 8 and 13 $\mu$m is so important to radiative cooling, I expected the control sample not to cool much, while the experimental samples would.

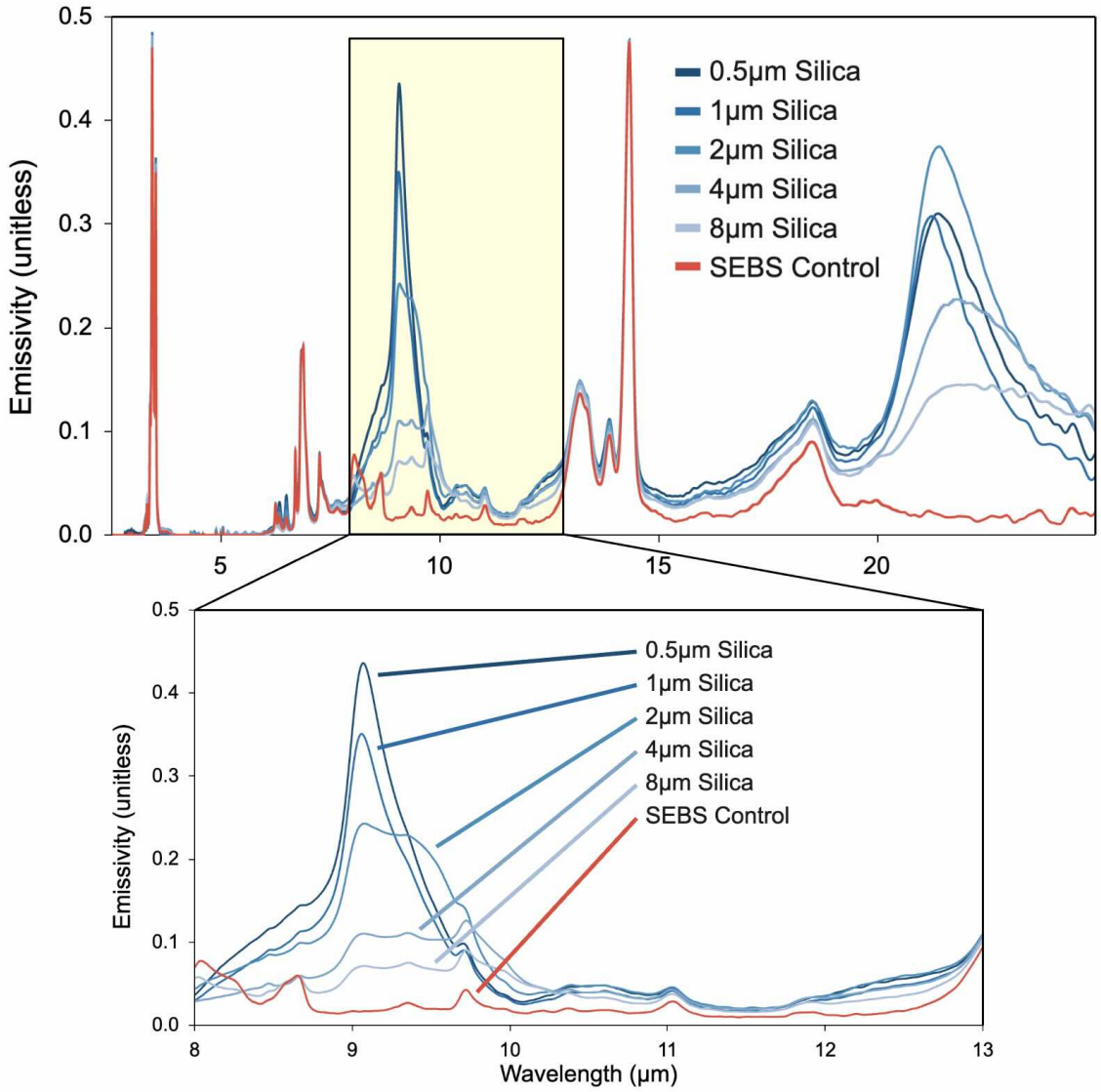


Figure 1.3: A graph of the upper bounds on the emissivities of my experimental and control samples.

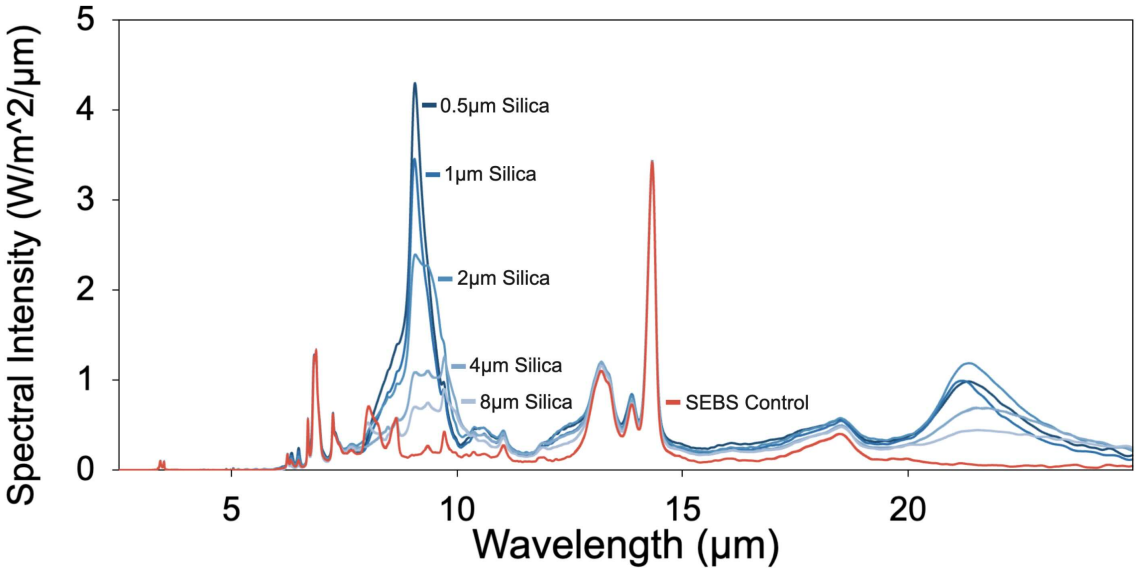


Figure 1.4: A graph of the upper bounds on the spectral intensities of my experimental and control samples at a temperature of 300 K.

Multiplying each emissivity spectrum by the 300-K blackbody curve (as in Equation 1.2), I found and plotted the upper bounds on the spectral intensities of each sample at 300 K in Figure 1.4. This calculation served as a rough rule of thumb for how I expected each sample to perform in cooling experiments. I expected the 0.5 $\mu$m sample to do the best and the SEBS control sample to do the worst. The peaks around 13 and 14 $\mu$m suggested that there might be a lesser, uniform cooling effect common to all of the samples, and I kept that in mind as I analyzed my experimental results in chapter 3.

All in all, the physics of radiative cooling are well-established, and the phenomenon has promise for satisfying the demand for electricity-free air conditioning. In chapter 2, I performed steady-state Python simulations to guide my experimental planning and design.

# Chapter 2

# Steady-State Python Simulations of Heat Transfer

## 2.1 How they Work

When heat transfers into or out of a solid, its temperature increases or decreases in response. The object's heat capacity determines how much its temperature changes in response to a given amount of heat. However, if the net heat transfer (the difference between the heat transfer into the solid and the heat transfer out of the solid) is zero, then the temperature change will be zero, regardless of the object's heat capacity. This means that predicting an object's equilibrium or steady-state temperature in a given environment is simpler than predicting its exact function of temperature over time. My simulations predict the steady-state temperatures of samples by finding the temperature at which the rate of heat transfer into the sample equals the rate of heat transfer out of the sample. Since the rates of heat transfer in my experiments were only dependent on the instantaneous temperatures of a sample and its environment (without any hysteresis), this calculation was possible without knowing the heat capacity of the samples.

My simulations used iteration to find the steady-state temperatures of samples. They began with a rough estimate of the steady-state temperature of the sample (for this, they used the ambient temperature of the sample's environment), then they

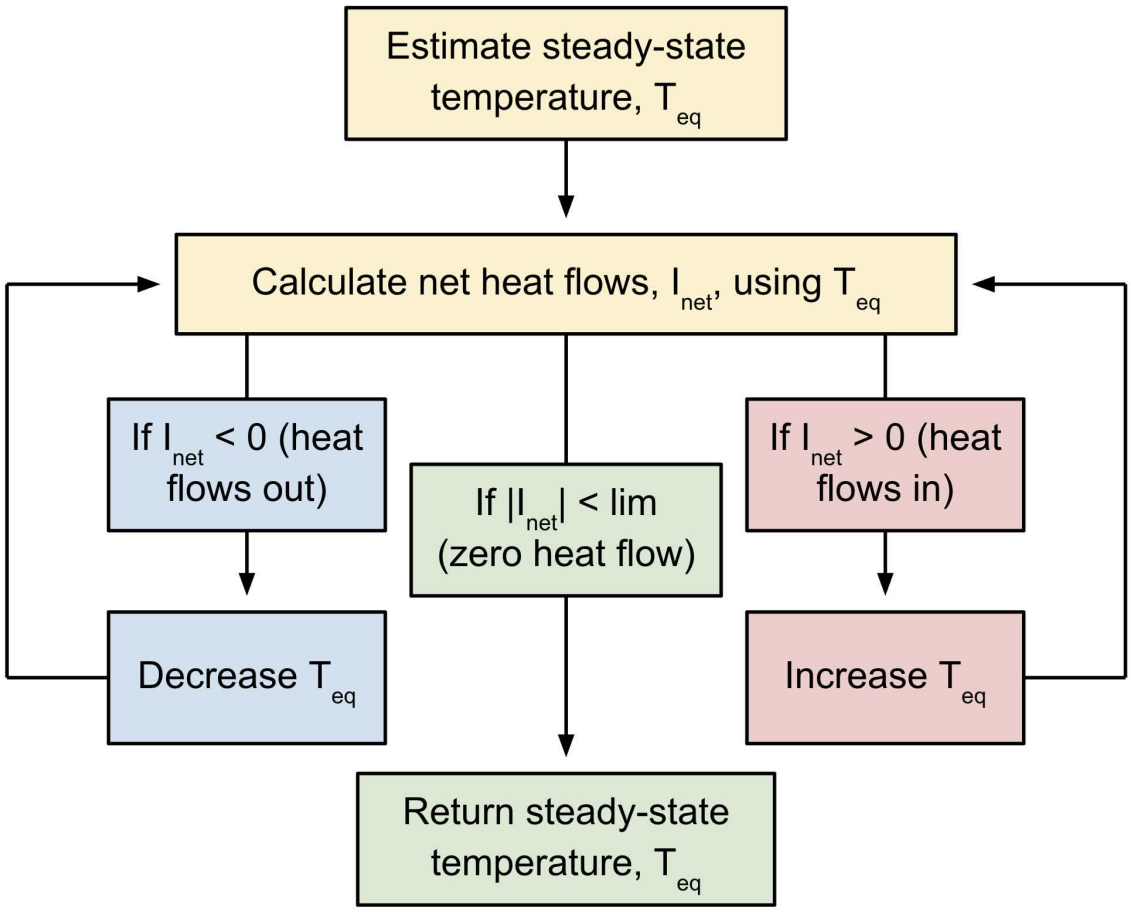


Figure 2.1: A diagram of the iterative logic used in my steady-state Python simulations.

calculated the rate of heat transfer into or out of the sample, and they updated their temperature estimates based on whether the net heat transfer was into or out of the sample. If the net heat transfer was out of the sample, my simulation decreased its temperature estimate. If the net heat transfer was into the sample, my simulation increased its temperature estimate. If the net heat transfer was sufficiently close to zero, my simulation halted and reported its last estimate as the steady-state temperature of the sample. This flow of logic is depicted in Figure 2.1.

I created simulations for both daytime and nighttime radiative cooling. The daytime radiative cooling simulations calculated the contributions from four methods of heat transfer: solar radiation, radiative cooling, atmospheric radiation, and con-

ductive and convective transfers (explained further below). The nighttime radiative cooling simulations calculated the same contributions, excluding solar radiation, as the sun is not a factor at night.

### 2.1.1 Solar Radiation

Heat transfer by solar radiation is a heat flow into a sample due to light from the sun striking the surface of the sample and being absorbed by it. The intensity of this heat flow (heat absorbed per unit time per unit surface area) is dependent on the amount of solar radiation striking the sample and the absorptivity (or emissivity) of the sample. I used Equation 2.1 to calculate this source of heat transfer in my daytime radiative cooling simulations.

$$I_{\text{sun}} = \int_0^\infty I_{\text{sun,Earth},\lambda}(\lambda)\,\epsilon(\lambda)\,d\lambda \tag{2.1}$$

In Equation 2.1, $\epsilon(\lambda)$ is the absorptivity of the sample and $I_{\text{sun,Earth},\lambda}(\lambda)$ is specifically the spectral intensity of solar radiation received by a sample on Earth's surface exposed to direct sunlight, as graphed in Figure 1.2. It is not the same as the emission of the sun's surface, as might be calculated using Equation 1.2, because it has been attenuated by the inverse-square law as it traveled to Earth. Since the heating of the sample is dependent on the intensity of the light when it strikes the sample and not the intensity of the light when it left the sun, it would not be accurate to use Equation 1.2 to calculate $I_{\text{sun,Earth},\lambda}(\lambda)$. Instead, one might use Equation 2.2 to appropriately attenuate the sun's radiation.

$$I_{\text{sun,Earth},\lambda}(\lambda) = B_\lambda(\lambda, T)\cdot\epsilon(\lambda)\cdot\frac{R_{\text{sun}}^2}{d_{\text{Earth}}^2} \tag{2.2}$$

where $R_{\text{sun}}$ is the radius of the sun and $d_{\text{Earth}}$ is the distance of Earth from the sun. However, this step is unnecessary, as the National Renewable Energy Laboratory has already determined the spectral intensity of the solar radiation received by Earth [4].

### 2.1.2 Radiative Cooling

Heat transfer by radiative cooling is a heat flow out of a sample due to the radiation it emits. It is the only source of heat transfer in my simulations that is consistently outward, meaning that it is the only source of cooling. The intensity of this heat flow is dependent on the blackbody spectrum at the sample's temperature and the emissivity of the sample. I used Equation 2.3 to calculate this source of heat transfer in my simulations.

$$I_{\text{rad}} = \int_0^\infty B_\lambda \left(\lambda, T_{\text{eq}}\right) \epsilon \left(\lambda\right) d\lambda \tag{2.3}$$

where $B_\lambda \left(\lambda, T_{\text{eq}}\right)$ is the blackbody spectrum at the sample's steady-state temperature and $\epsilon \left(\lambda\right)$ is the sample's emissivity.

One simplification employed by Equation 2.3 is that it ignores the impacts of atmospheric attenuation on the rate of cooling. Atmospheric attenuation is the result of different wavelengths of light being absorbed by the air at different rates. This absorption can be characterized as exponential decay, or as attenuation in decibels per kilometer. Just as with solid objects, when the air absorbs light, it is heated by that light. Therefore, if a sample emits a lot of light at a strongly attenuated wavelength (which my samples do at the 13 and 14 $\mu$m spectral intensity peaks discussed in section 1.3 and plotted in Figure 1.4), that emission will only serve to heat the air around it. By heating the air around it, it will raise the temperature of its ambient environment, so it will not be able to cool as much as otherwise expected.

However, if the attenuation is weak enough, and if there is enough circulation in the air near the sample, then that heat should quickly be carried away from the sample, and its cooling should not be severely impacted by the attenuation. According to the plot of attenuation in Figure 2.2, the maximum attenuation of light in my wavelength region of interest (light with a wavelength between 2.5 $\mu$m and 25 $\mu$m) should be around 3000 dB/km. That is equivalent to a factor of ten reduction in the intensity of emitted light every 3 meters. In other words, 90% of the radiated heat is reabsorbed by the air within 3 meters of the sample. While that sounds like strong attenuation, it is important to remember that these simulations are modeling outdoor experiments, where the air is not stagnant. Only 10% of the radiated heat is reabsorbed within the first 15 centimeters, and at that point it

should be far enough away from the sample to be blown away by air circulation and wind. Indeed, I conducted a couple experiments where I added a fan to the experimental apparatus to see if the increased circulation impacted cooling, and there was not a significant change to the samples' cooling behaviors. Therefore, I am satisfied to ignore the impacts of atmospheric attenuation in my simulations.

### 2.1.3 Atmospheric Radiation

Heat transfer by atmospheric radiation is a heat flow into a sample due to light emitted by the atmosphere striking the surface of the sample and being absorbed by it. The intensity of this heat flow is dependent on the blackbody spectrum at air temperature, the emissivity spectrum of air, and the emissivity spectrum of the sample. I used Equation 2.4 to calculate this source of heat transfer in my simulations.

$$I_{\text{atm}} = \int_0^\infty B_\lambda \left(\lambda, T_{\text{atm}}\right) \epsilon_{\text{atm}} \left(\lambda\right) \epsilon \left(\lambda\right) d\lambda \tag{2.4}$$

where $B_\lambda \left(\lambda, T_{\text{atm}}\right)$ is the blackbody spectrum at the ambient (or air) temperature and $\epsilon_{\text{atm}} \left(\lambda\right)$ is the atmosphere's emissivity. The atmosphere, like any other substance, is constantly emitting thermal radiation at its own temperature and with its own characteristic emissivity. The samples absorb some of this light and heat up because of it.

### 2.1.4 Conductive and Convective Transfers

Heat transfer by conduction and convection are heat transfers into a sample due to the air and surfaces in contact with it. Ideally, these sources of heat transfer are kept to a minimum by the styrofoam test stands the samples are placed in during my experiments. This is why they are lumped together as one source of heat transfer and calculated simply using Newton's law of cooling (which predicts the rate of heat transfer to be proportional to the difference between the sample's temperature and the ambient temperature of its environment). Equation 2.5 describes how I calculated this source of heat transfer for my simulations.

$$I_{\text{con}} = H \left(T_{\text{atm}} - T\right) \tag{2.5}$$

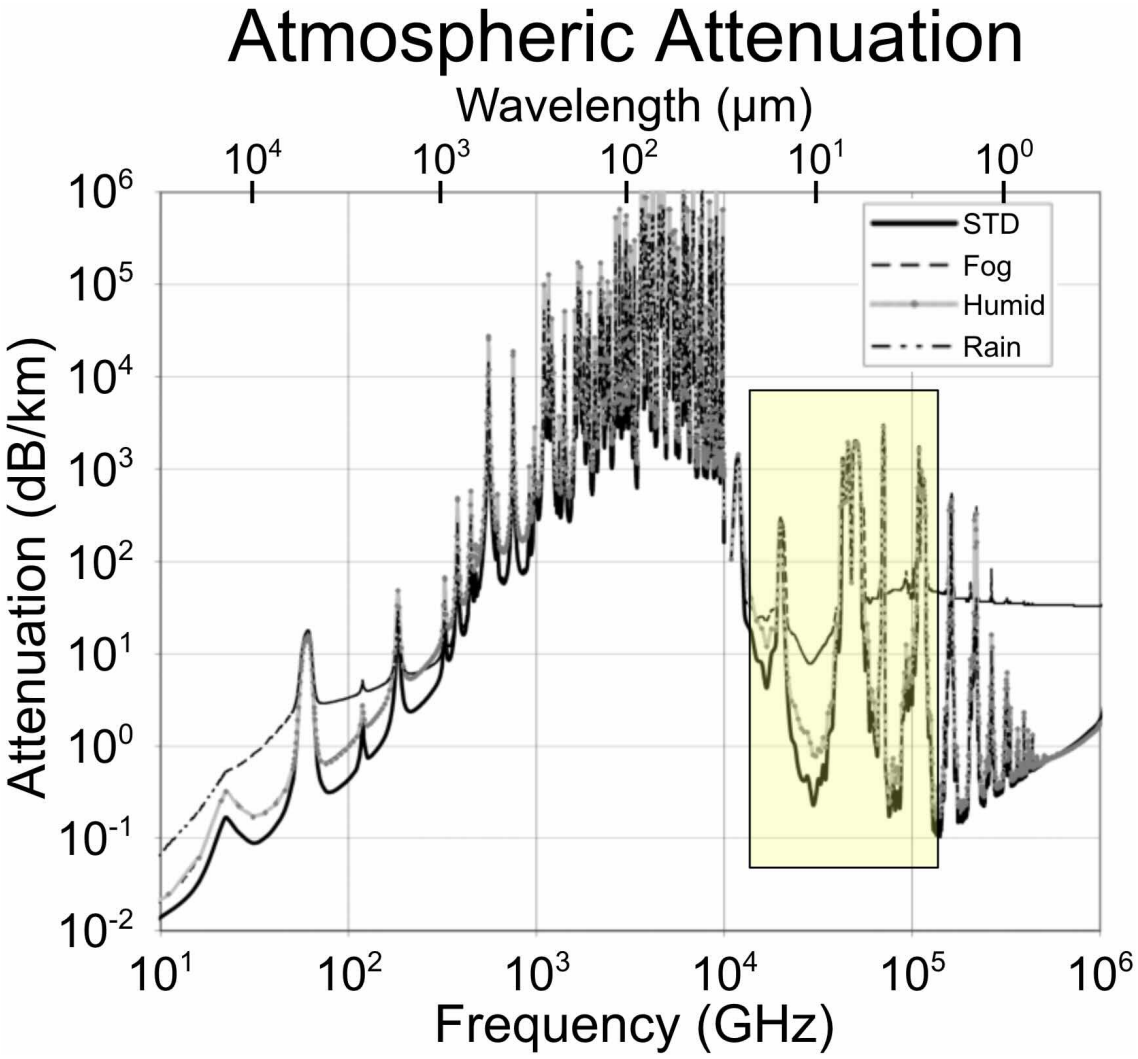


Figure 2.2: A graph of atmospheric attenuation at sea level by frequency and wavelength with my region of interest (wavelengths from 2.5 $\mu$m to 25 $\mu$m) highlighted [5].

where $H$ is the heat transfer coefficient between the sample and its environment. The heat transfer coefficient is a description of how connected or insulated a sample is with respect to its environment. A larger value of $H$ corresponds to a sample in close thermal contact with its environment, while a lower value of $H$ corresponds to a sample that is very insulated from its environment. I do not have a simple way to calculate or measure the heat transfer coefficient, but I do have an estimate of $H = 6.9\text{W/m}^2\text{/K}$ from a similar set of experiments where the samples should have been more insulated than mine were [6]. Therefore, $6.9\text{W/m}^2\text{/K}$ should serve as a rough lower bound on $H$ for my experiments.

### 2.1.5 The Big Picture

Each of these sources of heat transfer has a different relationship with the steady-state temperature, $T_{\text{eq}}$. Solar radiation is independent of $T_{\text{eq}}$, radiative cooling is dependent on $T_{\text{eq}}$ for its impact on a sample's blackbody spectrum, atmospheric radiation is independent of $T_{\text{eq}}$, and conductive and convective transfers are linearly dependent on $T_{\text{eq}}$. In my simulations, this means that solar radiation and atmospheric radiation do not have to be recalculated every time the steady-state temperature is updated, which saves computation time. Also, these relationships make it clear how and why the samples arrive at equilibrium. As can be seen in Figure 2.3, radiative cooling becomes less powerful as a sample cools, while conductive and convective transfers become more powerful. Eventually, conductive and convective transfers become powerful enough to prevent further cooling. Since these relationships are roughly linear, they produce a roughly linear relationship between $I_{\text{net}}$ and $T_{\text{eq}}$, as shown in Equation 2.6.

$$I_{\text{net}} \approx m\,(T_{\text{eq}} - T) \tag{2.6}$$

where $T_{\text{eq}}$ is the equilibrium temperature and $m$ is the slope. Since net heat transfer is proportional to the time derivative of temperature by the definition of heat capacity listed in Equation 2.7, the system's temperature is very nearly linear in

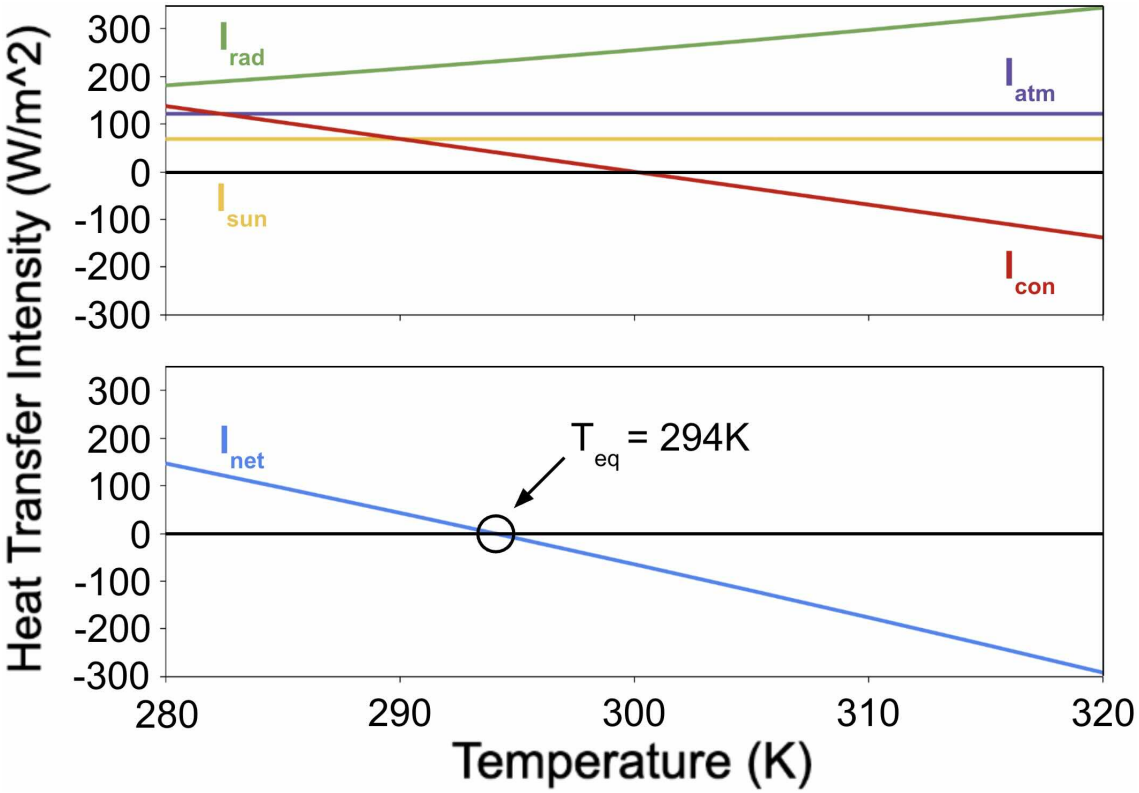


Figure 2.3: A graph of the intensity of the four sources of heat transfer (above) as well as the net intensity of heat transfer (below) versus temperature for a typical daytime simulation. The temperature-dependencies of $I_{\text{rad}}$ and $I_{\text{con}}$ lead to a roughly linear dependency for $I_{\text{net}}$. These data come from a simulation in section 2.2 with parameters $T_{\text{atm}} = 300\text{K}$, $H = 6.9\text{W/m}^2\text{/K}$, $\epsilon_s = 0.05$ (this parameter is introduced in section 2.2), and $\epsilon_t = 0.95$ (this parameter is also introduced in section 2.2).

its first derivative.

$$\frac{dT}{dt} = \frac{dQ}{dt} \cdot \left(\frac{dQ}{dT}\right)^{-1} = \frac{P_{\text{net}}}{C} = \frac{A}{C} \cdot I_{\text{net}} \approx \frac{A}{C} \cdot m\,(T_{\text{eq}} - T) \tag{2.7}$$

where $P_{\text{net}}$ is the power of net heat transfer, $A$ is the area of the sample, and $C$ is the heat capacity of the sample. This linearity suggests that the function of temperature over time should resemble exponential decay to solve the differential equation above. I use this fact in chapter 3 to analyze the time series temperature data I collected from the samples in my experiments.

## 2.2 Simulations to Probe Important Emissivity Regions

First, I conducted simulations of daylight conditions, so my simulations calculated the net heat transfer into the sample via Equation 2.8.

$$I_{\text{net}} = I_{\text{sun}} - I_{\text{rad}} + I_{\text{atm}} + I_{\text{con}} \tag{2.8}$$

where the four sources of heat transfer are calculated according to the equations derived in section 2.1. In order to investigate the importance of maximizing emissivity in the infrared atmospheric transparency window relative to the importance of minimizing the emissivity in the peak solar radiation range, I modeled the emissivity of the samples in this simulation as a tuneable piecewise function. This model took the emissivity in the 0.2 to 4 $\mu$m range to be a constant, $\epsilon_s$ (for solar radiation), the emissivity in the 8 to 13 $\mu$m range to be another constant, $\epsilon_t$ (for transparency window), and the emissivity at all other wavelengths to be zero, as shown in Equation 2.9.

$$\epsilon(\lambda) = \begin{cases} \epsilon_s & 0.2\mu\text{m} \leq \lambda \leq 4\mu\text{m} \\ \epsilon_t & 8\mu\text{m} \leq \lambda \leq 13\mu\text{m} \\ 0 & \text{otherwise} \end{cases} \tag{2.9}$$

Naturally, the optimal radiative cooling material would have $\epsilon_s = 0$ and $\epsilon_t = 1$, as those values would minimize absorption and maximize emission. Simulating samples with 10,000 combinations of $\epsilon_s$ and $\epsilon_t$, I produced the heatmap on the left in Figure 2.4.

This simulation confirmed my expectations that the optimal sample minimized absorption in the peak solar radiation range and maximized emission in the infrared atmospheric transparency window. However, it also showed that a high value of $\epsilon_s$, corresponding to a high value of a sample's emissivity in the peak solar radiation range, is incredibly detrimental to a sample's radiative cooling capabilities. Increasing $\epsilon_s$ by a step of 0.01 diminishes a sample's cooling capacity just as much as decreasing $\epsilon_t$ by a step of 0.1 (i.e. $\frac{\partial T_{eq}}{\partial \epsilon_s} \approx -10\frac{\partial T_{eq}}{\partial \epsilon_t}$ when evaluated at values $\epsilon_s << \epsilon_t$). This simulation implies that radiative cooling samples are incredibly

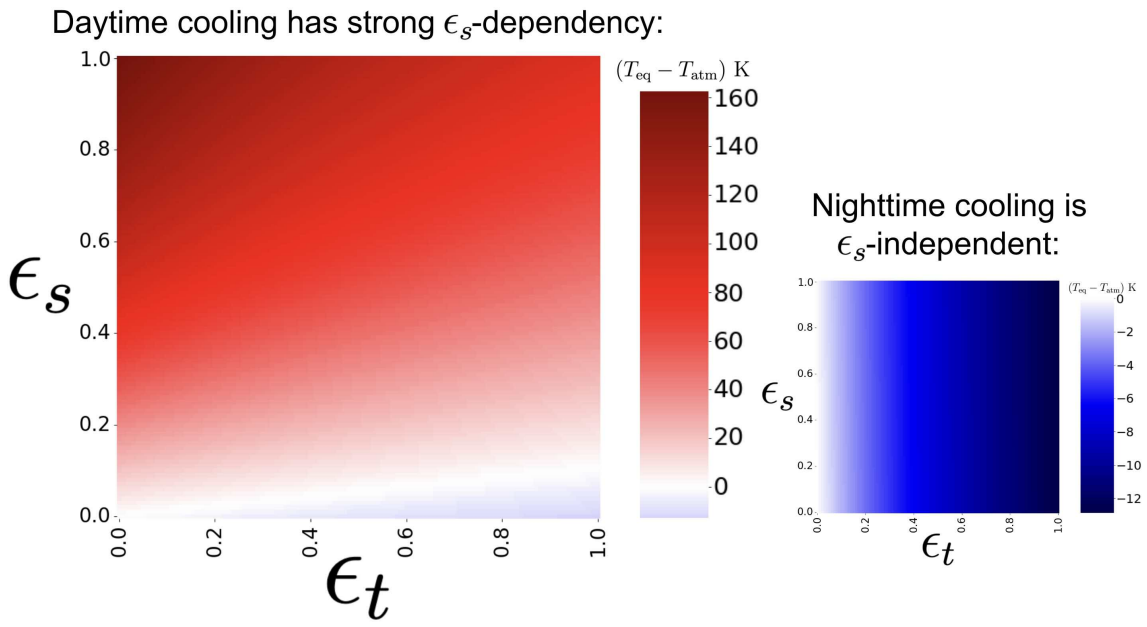


Figure 2.4: **Left**: A heatmap showing the difference between the steady-state temperature of a sample and the ambient air temperature of the daytime simulation (in this case $T_{\text{atm}} = 300\text{K}$) for 10,000 combinations of $\epsilon_s$ and $\epsilon_t$. This simulation used $H = 6.9\text{W/m}^2\text{/K}$. In the ideal case ($\epsilon_s = 0$ and $\epsilon_t = 1$), the temperature difference $T_{\text{eq}} - T_{\text{atm}}$ is $-12.7$ K. In the worst case ($\epsilon_s = 1$ and $\epsilon_t = 0$), the temperature difference is 162.6 K. **Right**: A heatmap showing the results of the same simulation in a nighttime environment. In the ideal case ($\epsilon_s = 0$ and $\epsilon_t = 1$), the temperature difference $T_{\text{eq}} - T_{\text{atm}}$ is $-12.8$ K. In the worst case ($\epsilon_s = 1$ and $\epsilon_t = 0$), the temperature difference is $-0.2$ K.

sensitive to their emissivity values in the peak solar absorption range, which makes it difficult to determine the impact that infrared window emissivities have on a sample's temperature during the day. Variations in solar range emissivities would simply create too much noise for the infrared window emissivities to produce a clear trend in experiments.

Running the same simulation for a nighttime environment, I simply altered Equation 2.8 by removing $I_{\text{sun}}$ from the sum. This simulation produced the right panel in Figure 2.4, which includes a heatmap much more conducive to determining the impact that emissivities in the infrared atmospheric transparency window have on radiative cooling. At night, the simulation predicts that the steady-state temperature is almost completely independent of $\epsilon_s$.

Given these predictions, as well as some preliminary results from daytime experiments, I decided to focus my research on nighttime experiments. That way, I could more accurately determine the impact that the different infrared window emissivity profiles of the different samples were having on how much each sample cooled.

## 2.3 Simulations to Predict the Performance of Experimental and Control Samples at Night using FTIR Data

Having decided to focus on nighttime measurements, I simulated nighttime radiative cooling based on the Fourier-transform infrared spectroscopy (FTIR) data discussed in section 1.3. Since the FTIR data spans the range from 2.5 to 25 $\mu$m, this type of simulation is limited to nighttime radiative cooling for now, because accurately modeling solar radiation requires sample emissivity data down to wavelengths around 0.2 $\mu$m, which I do not have. As discussed in section 1.3, the FTIR data provided me with upper bounds on sample emissivities and spectral intensities, which allows me to calculate upper bounds on radiative cooling intensities, $I_{\text{rad}}$, for each sample. Since radiative cooling is the only source of heat transfer out of the sample (as atmospheric radiation, $I_{\text{atm}}$, and conductive and convective transfers, $I_{\text{con}}$, both transfer heat into the sample), these upper bounds can be translated

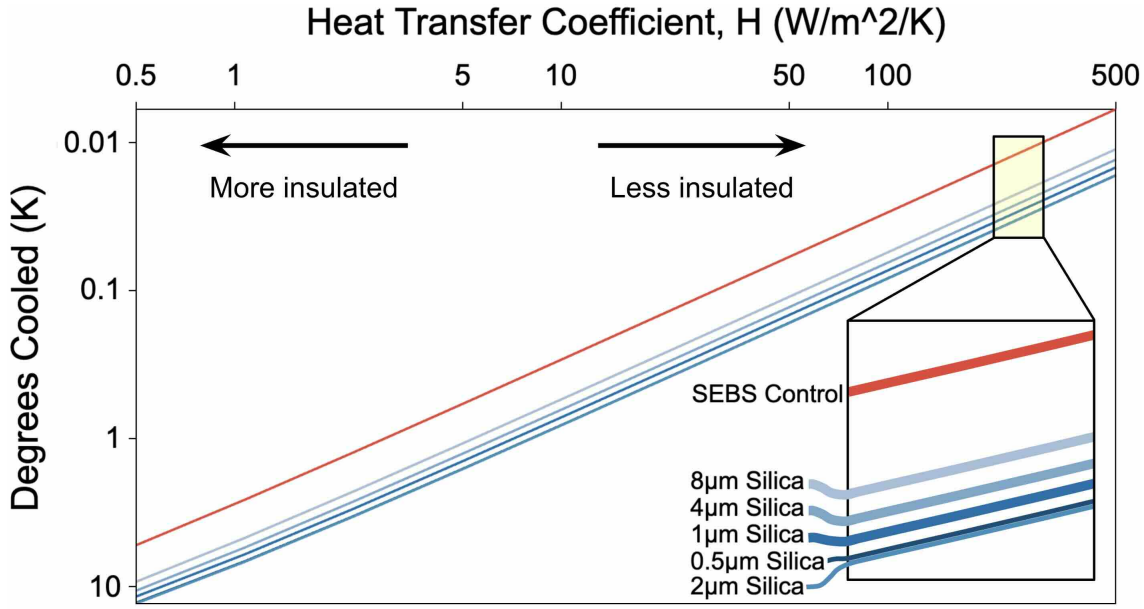


Figure 2.5: A log-log plot showing the lower bound on the steady-state cooling of each sample relative to the ambient temperature, $T_{\text{atm}} = 300\text{K}$, versus the heat transfer coefficient, $H$. The legend shows the samples in order of which get the coolest, and which remain the hottest.

into lower bounds on the steady-state temperatures that the samples can attain. I simulated these lower bounds for each sample for a variety of values of the heat transfer coefficient, $H$, and plotted the results in Figure 2.5.

Surprisingly, the 2 $\mu$m sample narrowly beat the 0.5 $\mu$m sample for cooling, but the rest of the ordering was as expected, with the control sample cooling the least. A noticeable feature of Figure 2.5 is that the curves for each sample are roughly parallel. On a log-log plot, parallel lines indicate that there is a constant ratio between the series. Therefore, these data indicate that the 8 $\mu$m sample should cool roughly 1.8 times as much as the control sample (i.e. $\frac{T_{\text{eq},8}-T_{\text{atm}}}{T_{\text{eq,c}}-T_{\text{atm}}} = 1.8$), regardless of the value of the heat transfer coefficient, $H$. Likewise, the 2 $\mu$m sample should cool 2.8 times as much as the control sample (i.e. $\frac{T_{\text{eq},2}-T_{\text{atm}}}{T_{\text{eq,c}}-T_{\text{atm}}} = 2.8$), regardless of $H$. I plotted the cooling ratios between each sample and the control sample in Figure 2.6. As you can see, they are roughly independent of $H$, but they start to decrease as $H$ gets very small. For my purposes, this means that the ratio should be constant,

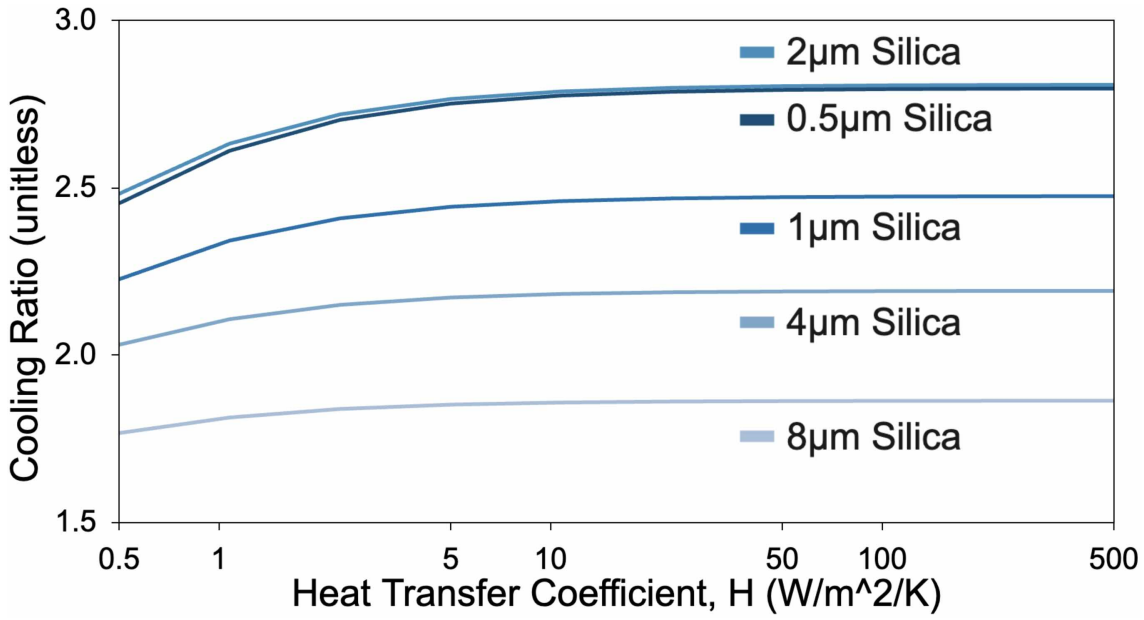


Figure 2.6: A semi-log plot showing the predicted value of the ratios between the cooling of the experimental samples and that of the control sample, $\frac{T_{\mathrm{eq,e}}-T_{\mathrm{atm}}}{T_{\mathrm{eq,c}}-T_{\mathrm{atm}}}$. These data come from the same simulation as the data in Figure 2.5.

because it is unlikely that my experiments were so well-insulated as to have a value of $H < 6.9\mathrm{W/m^2/K}$ (as discussed in subsection 2.1.4).

These ratios are not necessarily predictive of actual cooling data since they are derived from a lower bound on temperature. One or all of the samples' experimental steady-state temperatures could be far above its lower bound (i.e. far less effective at cooling), which might skew these ratios up or down. Still, regardless of the values these ratios hold, they should still be independent of $H$, as predicted in this simulation. Therefore, they are still relevant to pay attention to in experimental data. While $H$ is likely to change with weather conditions, quantities like the spectral intensities of the samples (the quantities that these ratios are more dependent on) are less likely to change from night to night.

Taken together, my simulations guided me toward nighttime experiments and gave me insights on what to pay attention to in the resultant data. My simulations justified the use of exponential fits on temperature time series (due to the approximate linearity of the heat transfer in Figure 2.3) as well as a focus on the

ratios between the amount of cooling attained by each sample. They were incredibly informative for me as I began conducting the experiments detailed in chapter 3.

# Chapter 3

# Side-by-Side Nighttime Experiments

## 3.1 Experimental Methods

I tested the efficacy of my SEBS radiative cooling samples by exposing them to the night sky and measuring the response of their temperatures over time (specifically, over periods of 30 to 45 minutes). The tests were conducted in two side-by-side test stands: one for the experimental sample and one for the control sample. As depicted in Figure 3.1, the samples each sat on an aluminum plate on top of a styrofoam test stand with a thermocouple placed between the sample and the metal. In later tests, the thermocouple would be placed underneath the aluminum in order to compare the cooling of the SEBS control sample to that of the bare aluminum plate. This arrangement is referenced later in Figure 3.5.

## 3.2 Analytical Methods

As introduced in subsection 2.1.5, the net heat transfer of the samples should be roughly linearly dependent on their temperatures. Since heat transfer is proportional to the rate of change of a sample's temperature, and since $I_{\text{net}}$ is described by a linear relationship with some slope, $m$, and equilibrium temperature, $T_{\text{eq}}$, the temperature

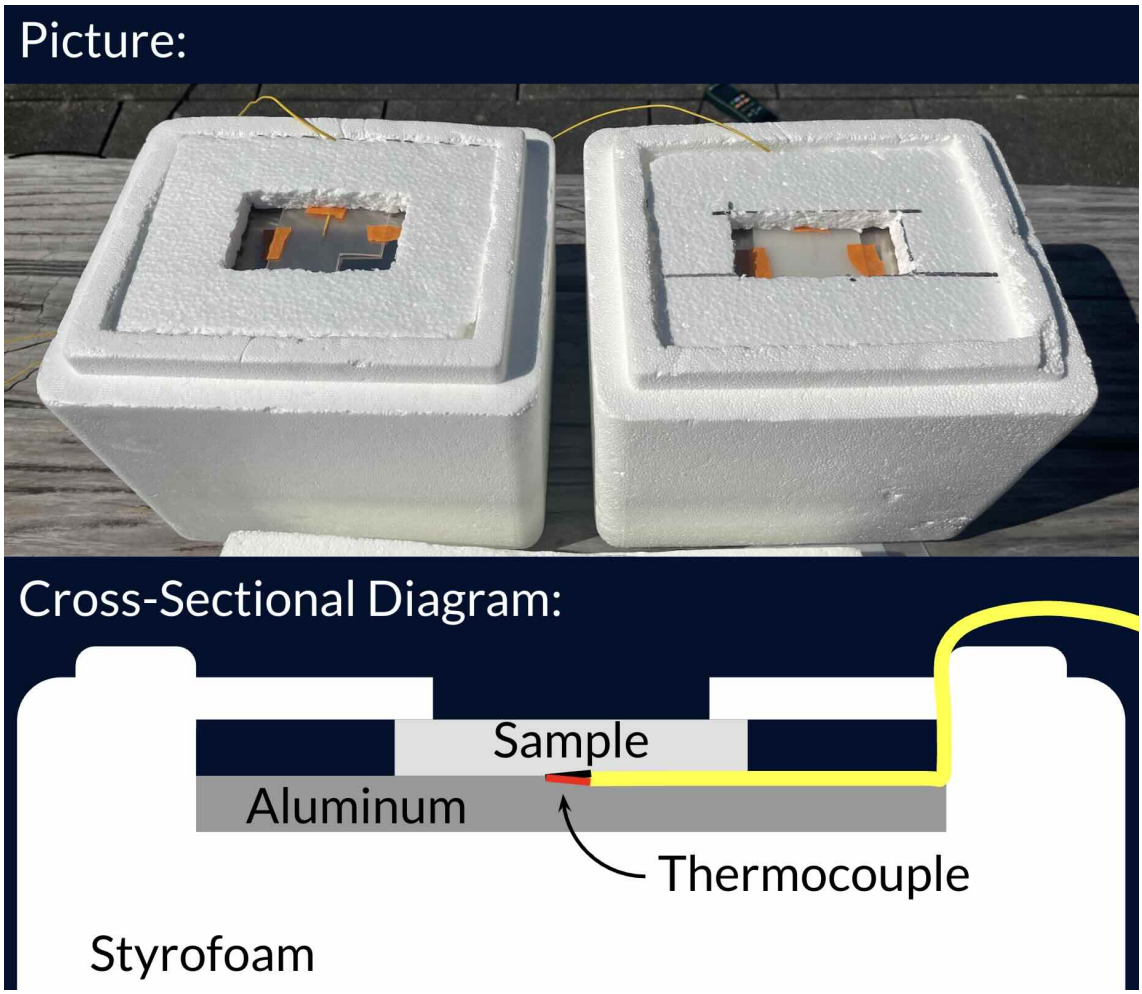


Figure 3.1: A picture and a diagram depicting the arrangement of the samples for my first round of night measurements comparing experimental samples to the control sample.

of a sample over time should roughly follow the exponential decay curve shown in Equation 3.1.

$$T(t) \approx Ae^{-\frac{t}{\tau}} + T_{\text{eq}} \tag{3.1}$$

where $A$ is the displacement of the sample temperature from equilibrium at the start of the experiment, $\tau$ is a time constant describing the rate of decay, and $T_{\text{eq}}$ is the steady-state temperature of the sample.

I applied this exponential fit to all my temperature time series, except for those in which the fit predicted that $A$ was either less than 2 K or greater than 25 K (in which case the fit failed). $A$ should not be greater than 25 K, because that would imply a cooling capacity far beyond what was predicted by the simulations in chapter 2. I also rejected fits where $A < 2\text{K}$, because such a small initial displacement suggests that the sample was already within two degrees of its equilibrium temperature at the start of the experiment. Starting so close, a simple mean of the last ten minutes of data should be sufficient to estimate $T_{\text{eq}}$. Fits tended to fail (in either direction, high $A$ or low $A$) when a sample's temperature started off very close to its equilibrium temperature, as being so close to the equilibrium meant that fluctuations due to noise and weather changes dominated any trend in the data. Whenever a fit failed, I chose to estimate $T_{\text{eq}}$ with the mean of the temperature over the last ten minutes of the measurement period.

In order to estimate the uncertainty in my measurements, I took the residuals of the time series with respect to the exponential fit over the last ten minutes of the measurement period (or, if the fit failed, I took the residuals with respect to the mean of the last ten minutes). Then, I computed the square root of the sum of the squares of the residuals and used that number as the uncertainty in my estimate of $T_{\text{eq}}$. Figure 3.2 shows an example of what a sample's temperature time series looks like, what its exponential fit looks like, and what its steady-state temperature estimate looks like.

## 3.3 Sample versus Sample

In the first round of experiments, I compared the cooling capacity of the experimental samples to that of the control sample, expecting the experimental samples to cool

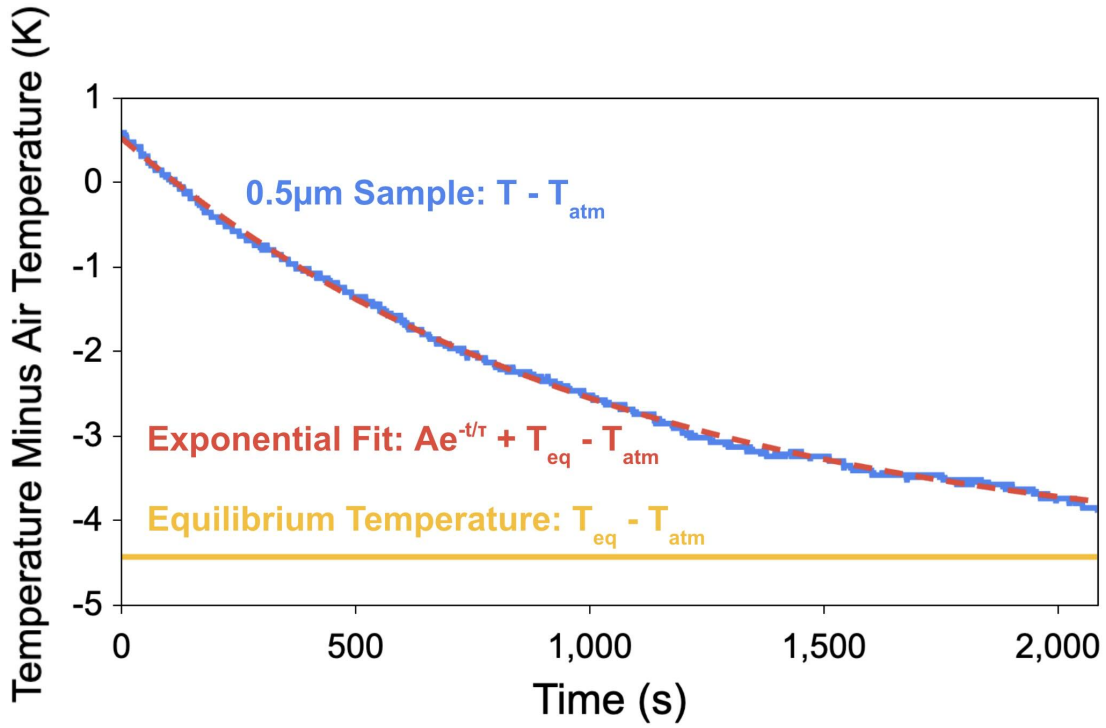


$$A = 5.24\text{K} \qquad \tau = 1213\text{s} \qquad T_{\text{eq}} - T_{\text{atm}} = -4.43\text{K}$$

Figure 3.2: A graph of temperature time series data taken for the 0.5 $\mu$m silica sample on November 12th, 2024, along with its exponential fit and steady-state temperature estimate. This is the method by which I estimated steady-state temperatures in all my experiments.

much more than the control sample based on my simulations in chapter 2. Instead, I found that the experimental and control samples cooled to a comparable degree in each side-by-side test. The greatest variation in cooling came from variable weather conditions, as the samples cooled to different temperatures on each of the six nights I measured them. The steady-state temperatures of the samples relative to the air temperature in each experiment are plotted in Figure 3.3 in chronological order of when the experiment was conducted. In the lower panel of the figure, I included a table of some of the salient weather conditions on each of these nights. While it is clear that the results of these experiments varied due to weather conditions, it is unclear what conditions lead to which result, as there is no clear relationship between a weather metric and the amount of cooling attained on a given night.

I also took a look at the ratios of the amount of cooling attained by the experimental samples relative to that of the control sample, $\frac{T_{\mathrm{eq,e}}-T_{\mathrm{atm}}}{T_{\mathrm{eq,c}}-T_{\mathrm{atm}}}$. As detailed in section 2.3, my simulations predicted that the experimental samples should cool roughly 1.8 to 2.8 times more than the control sample and that this ratio should be fairly independent of the heat transfer coefficient, $H$. This means that each experimental sample should have one value for its cooling ratio and stick to it regardless of weather conditions. Therefore, I found it incredibly surprising that the variation in this metric was also better explained by weather variations than by which sample was being measured, as can be seen in Figure 3.4. Also, the fact that the actual ratios are much smaller than those predicted by the simulation in section 2.3 suggests that the emissivities of the experimental samples must be much lower than the upper bounds described in that section, while the emissivity of the control sample should be closer to its upper bound. This means that the addition of the silica beads to the SEBS polymer might be much less effective at increasing the emissivity than expected.

A quantitative measure of which grouping of the experiments—by date or by sample—is more significant for explaining these results is an analysis of variance (ANOVA) test. This test determines how predictive a given grouping of the data is of the variance of the data. It does so by comparing the variance between groups to

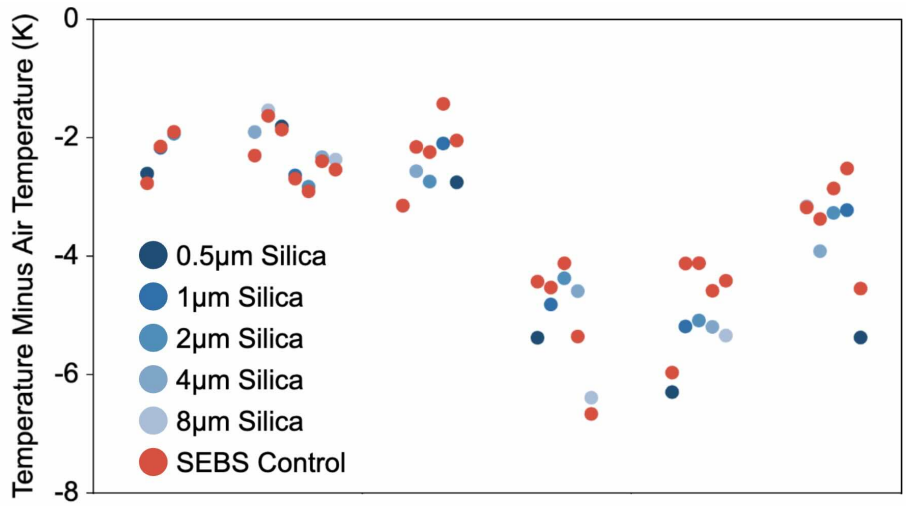


| Midnight conditions | 10/27 | 10/29 | 11/10 | 11/12 | 11/19 | 11/20 |
|---|---|---|---|---|---|---|
| Air Temp. (K) | 295 | 298 | 294 | 290 | 291 | 286 |
| Dew Point (K) | 293 | 295 | 293 | 286 | 283 | 271 |
| Wind Speed (kph) | 8 | 16 | 8 | 0 | 13 | 13 |

Figure 3.3: A graph of the steady-state temperatures of experimental and control samples on six different nights (above) and a table of important weather conditions at midnight on each night (below). The tests are plotted in chronological order and separated by which night they occurred on. The results vary significantly from night to night, but they are fairly similar over the span of a single night.

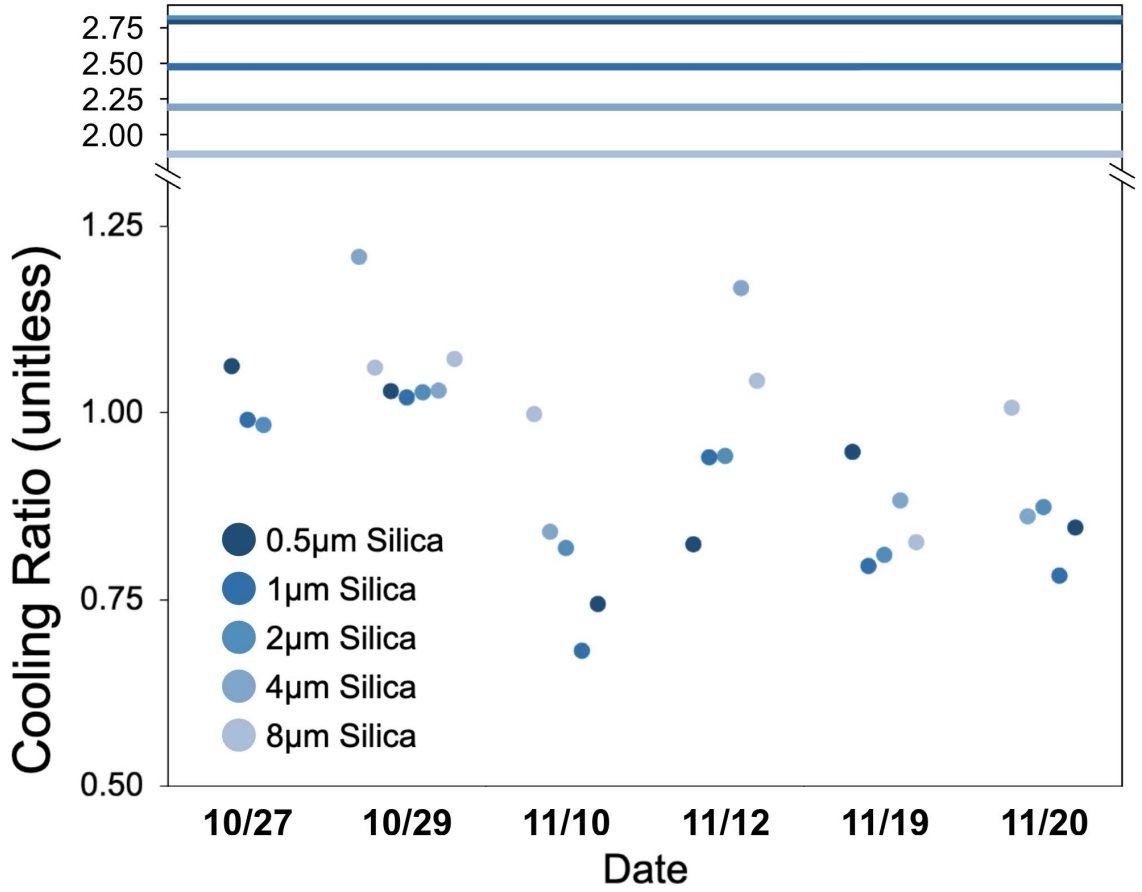


Figure 3.4: A graph of the ratios between experimental sample cooling and control sample cooling, $\frac{T_{\mathrm{eq,e}}-T_{\mathrm{atm}}}{T_{\mathrm{eq,c}}-T_{\mathrm{atm}}}$, on six different nights. The ratios predicted by the simulation in section 2.3 are the lines plotted above. The ratios are plotted in chronological order and separated by which night they occurred on. The results seem to vary from night to night, although that appearance is not as conclusive as the variation of the absolute temperature decreases in Figure 3.3.

the variance within groups via the $F$-statistic in Equation 3.2.

$$F = \frac{\text{variance between groups}}{\text{variance within groups}} = \frac{SS_{\text{between}}/(G-1)}{SS_{\text{within}}/(N-G)} \tag{3.2}$$

where $SS_{\text{between}}$ is the sum of squares of the group means minus the total mean, $SS_{\text{within}}$ is the sum of squares of each observation minus its appropriate group mean, $G$ is the number of groups, and $N$ is the number of observations. If a grouping has a low $F$-statistic, it means that the grouping does little to explain the variance of the data. For instance, if I were to randomly assign each experiment to a group, that grouping should have a low $F$-statistic. If the $F$-statistic is large, on the other hand, it means that the data is well-grouped, because the denominator, which corresponds to the variance of data within each group, is relatively small.

However, the $F$-statistic is not just dependent on the quality of a grouping. It is also dependent on the number of groups, $G$, and the number of observations, $N$. Therefore, it is necessary to extract a $p$-value from the $F$-statistic to compare groupings involving different numbers of groups (i.e. when $G_1 \neq G_2$). A $p$-value represents the probability that the data would be distributed as it is given that the null hypothesis (that the group means are all the same) is correct. This can be thought of as the probability of observing what I observed if the groupings were assigned at random. The smaller the $p$-value, the less plausible it is that the groupings could be random. Therefore, the grouping with more predictive power should be the one with a smaller $p$-value. Calculating the $p$-value can be accomplished by integrating over the probability density of the $F$-distribution. The $F$-statistic is distributed according to the $F$-distribution, which is dependent on the degrees of freedom $G-1$ and $N-G$. I performed the appropriate calculations to find values for $F$ and $p$ for each grouping of the data. I listed the results of my ANOVA tests on the absolute temperature decreases and on the experimental to control cooling ratios in Table 3.1.

For both the temperature decrease and the cooling ratio, the groupings by date had a lower $p$-value. While the groupings of cooling ratios by date still had a fairly high $p$-value of 0.335 (the typical cutoff for significance is 0.05), it was still smaller than that for the groupings by sample, meaning that even if the date is not a good predictor of the cooling ratio, knowing which experimental sample is being measured

| Grouping | Metric | $G$ | $N$ | $F$-statistic | $p$-value |
|---|---|---|---|---|---|
| By date | Temperature decrease ($T_{\text{eq}} - T_{\text{atm}}$) | 6 | 60 | 4.03 | **0.0035** |
| By sample | Temperature decrease ($T_{\text{eq}} - T_{\text{atm}}$) | 6 | 60 | 0.046 | 0.999 |
| By date | Cooling ratio $\frac{T_{\text{eq,e}} - T_{\text{atm}}}{T_{\text{eq,c}} - T_{\text{atm}}}$ | 6 | 30 | 1.21 | **0.335** |
| By sample | Cooling ratio $\frac{T_{\text{eq,e}} - T_{\text{atm}}}{T_{\text{eq,c}} - T_{\text{atm}}}$ | 5 | 30 | 0.23 | 0.917 |

Table 3.1: A summary table of my analysis of variance (ANOVA) tests on groupings by date and groupings by sample for the distribution of the temperature decreases and that of the cooling ratios. The grouping with the lower $p$-value is emphasized in bold, indicating that it is the one with more predictive power.

is an even worse predictor.

Therefore, these experiments demonstrated that weather variations from night to night are much more important in determining how much a sample will cool than what type of sample it is. Even the control sample seemed to cool a similar amount as the experimental samples. Both of these results were unexpected based on my simulations. In order to investigate them further, I decided to perform experiments comparing these SEBS samples to bare aluminum plates.

## 3.4 Sample versus Aluminum

In order to investigate the cooling capacity of the SEBS polymer, I compared the experimental and control samples to the bare aluminum plates they sat on according to the configuration depicted in Figure 3.5. If the SEBS polymer has its own cooling capacity as I suspect, then there should be a significant difference in how much it cools relative to the aluminum plates. I graphed the temperature decrease data for these experiments in Figure 3.6, and I graphed the ratios between the experimental samples' or aluminum plates' temperature decrease and that of the control sample in Figure 3.7. As you can see, the difference between the aluminum plates and the SEBS samples is much more noticeable than the differences between the experimental and control samples, suggesting that there is a significant cooling effect due to the SEBS polymer that the aluminum plates do not possess.

The analysis of variance (ANOVA) tests I conducted on these data reinforce the

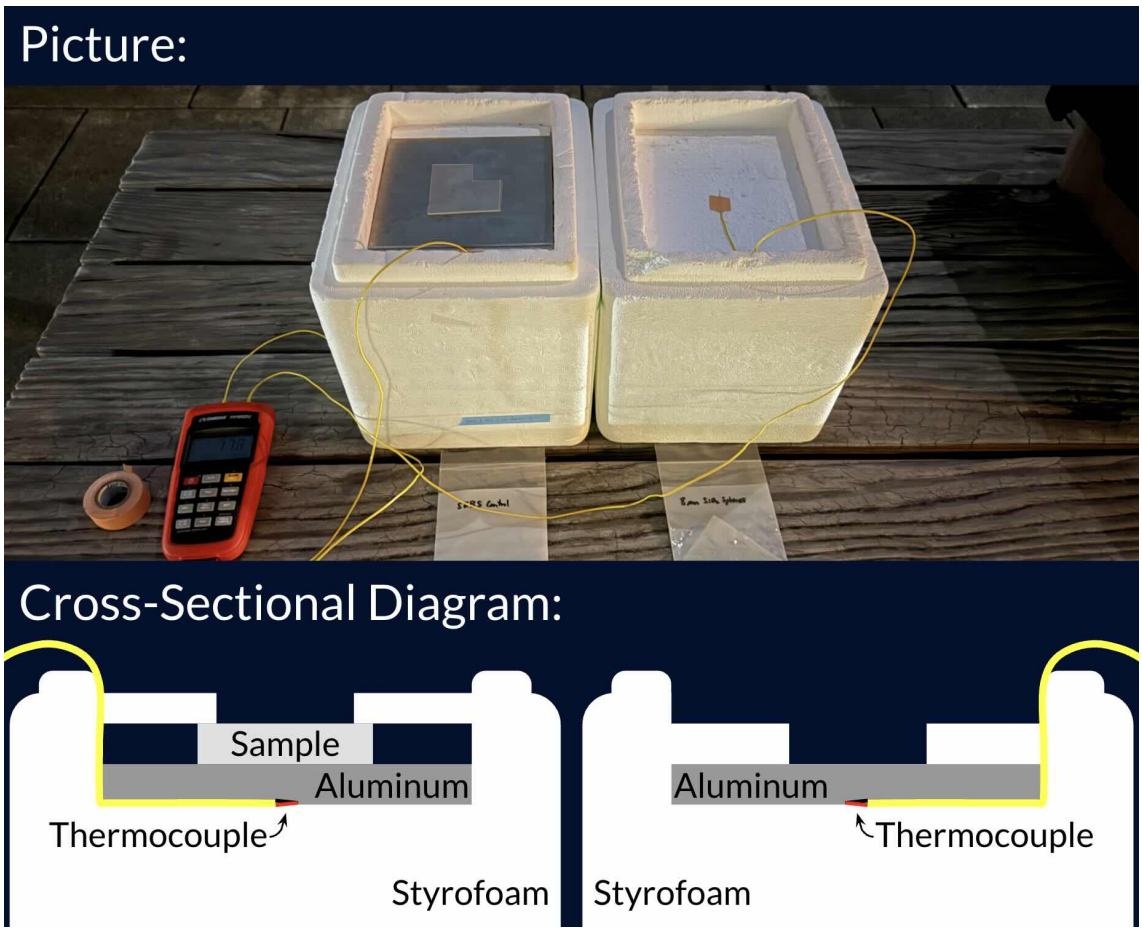


Figure 3.5: A picture and a diagram depicting the arrangement of the samples for my second round of night measurements comparing samples to bare aluminum plates.

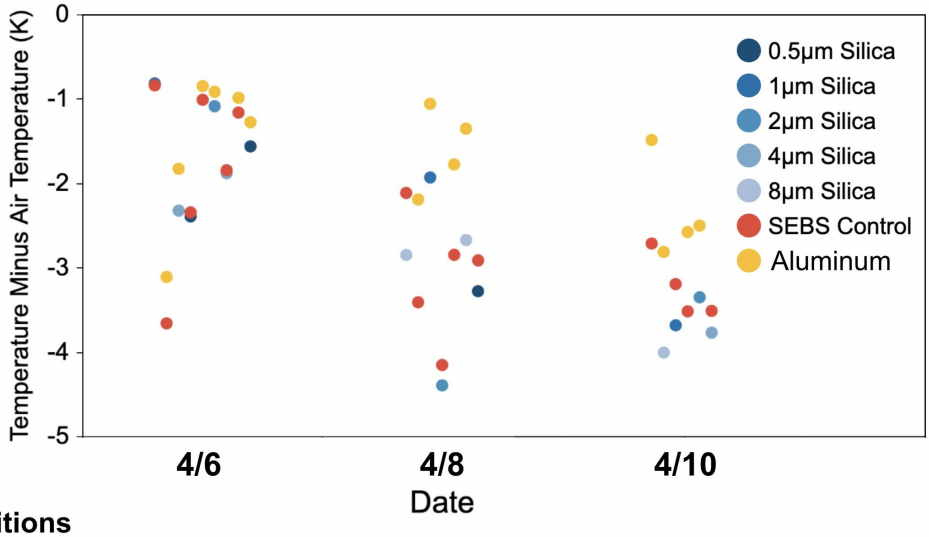


| Midnight conditions | | | |
|---|---|---|---|
| **Air Temp. (K)** | **283** | **288** | **293** |
| **Dew Point (K)** | **276** | **280** | **289** |
| **Wind Speed (kph)** | **24** | **15** | **8** |

Figure 3.6: A graph of the steady-state temperatures of SEBS samples and aluminum plates on three different nights (above) and a table of weather conditions at midnight on these nights (below). The tests are plotted in chronological order and separated by which night they occurred on. The results vary somewhat from night to night, but the more noticeable detail is that the aluminum plates cooled less than the SEBS samples they were compared to in each case.

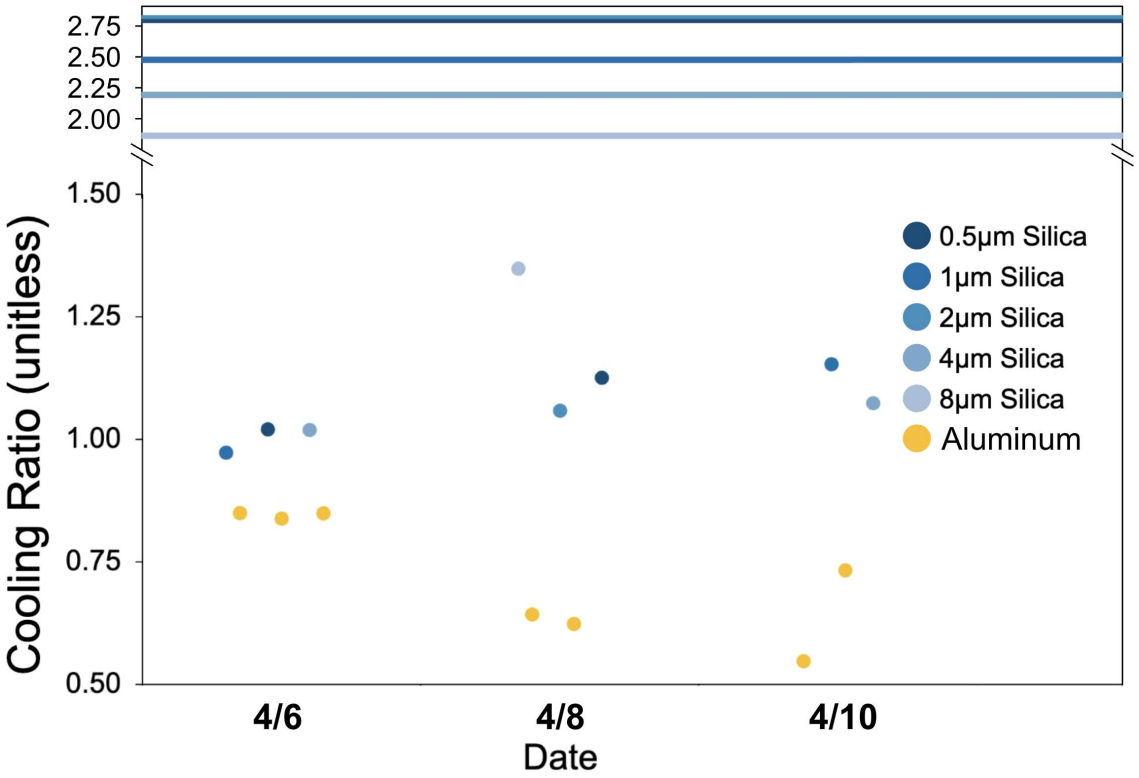


Figure 3.7: A graph of the ratios between experimental sample cooling or aluminum plate cooling and control sample cooling, $\frac{T_{\mathrm{eq,e}}-T_{\mathrm{atm}}}{T_{\mathrm{eq,c}}-T_{\mathrm{atm}}}$ or $\frac{T_{\mathrm{eq,a}}-T_{\mathrm{atm}}}{T_{\mathrm{eq,c}}-T_{\mathrm{atm}}}$, on three different nights. The ratios are plotted in chronological order and separated by which night they occurred on. The ratios predicted by the simulation discussed in section 2.3 are the lines plotted above. The results seem to vary significantly depending on if the ratio was between an experimental sample and the control sample or between an aluminum plate and the control sample.

| Grouping | Metric | $G$ | $N$ | $F$-statistic | $p$-value |
|---|---|---|---|---|---|
| By date | Temperature decrease ($T_{\text{eq}} - T_{\text{atm}}$) | 3 | 22 | 0.34 | 0.714 |
| By type (experimental, control, aluminum) | Temperature decrease ($T_{\text{eq}} - T_{\text{atm}}$) | 3 | 22 | 0.13 | 0.883 |
| By date | Cooling ratio $\frac{T_{\text{eq,e}} - T_{\text{atm}}}{T_{\text{eq,c}} - T_{\text{atm}}}$ or $\frac{T_{\text{eq,a}} - T_{\text{atm}}}{T_{\text{eq,c}} - T_{\text{atm}}}$ | 3 | 14 | 0.028 | 0.973 |
| By type (experimental, control, aluminum) | Cooling ratio $\frac{T_{\text{eq,e}} - T_{\text{atm}}}{T_{\text{eq,c}} - T_{\text{atm}}}$ or $\frac{T_{\text{eq,a}} - T_{\text{atm}}}{T_{\text{eq,c}} - T_{\text{atm}}}$ | 2 | 14 | 4.35 | **0.059** |

Table 3.2: A summary table of my analysis of variance (ANOVA) tests on groupings by date and groupings by type (experimental sample, control sample, or aluminum plate) for the distribution of the temperature decrease and that of the cooling ratios. The grouping with the lower $p$-value is in bold, indicating that it is the one with more predictive power.

idea that the SEBS polymer has some cooling capacity that the aluminum does not. While there was not much variation from night to night this time, there was variation between the experimental samples and the aluminum plates when looking at the cooling ratios between them and the control sample, as implied by the low $p$-value for the last row of Table 3.2. This means that grouping the cooling ratios by whether a SEBS sample was being measured against the control sample or whether an aluminum plate was being measured against the control sample was a strong predictor of the cooling ratio.

In total, the experiments detailed in this section and section 3.3 suggest that weather variations contribute more to cooling than the size and presence of silica beads in a SEBS sample and that the SEBS polymer itself has significant cooling properties that aluminum does not have. In chapter 4, I discuss some explanations for why this might be.

# Chapter 4

# Results and Discussion

## 4.1 Reasons for Variations due to Weather

The variations in sample temperature differences due to weather variations are simply explained by varying values of the heat transfer coefficient, $H$. Variables like temperature and humidity impact air circulation, which impacts how close the thermal contact is between the samples and their environment. However, variations in $H$ do not explain the variations in the cooling ratios observed in Figure 3.4. My simulations in Figure 2.5 suggested that the ratios between the cooling of each sample should be roughly constant with $H$. Therefore, variations in the cooling ratio must be a result of variations in the radiative cooling power of the samples. Increased humidity reduces the transparency of the infrared atmospheric transparency window. If decreased enough, atmospheric attenuation could become a concern, and my model assumption to ignore it (discussed in subsection 2.1.2 would be invalid). One way to determine if this is the case would be to introduce more temperature measurements into the experiments. Including a thermocouple a few centimeters away from the samples could help determine if the samples are creating a heated pocket of air due to atmospheric attenuation.

There could also be an issue with the way I have been measuring the air temperature around the samples. I have been using data from Dr. Everitt's weather station near Rice University to measure the temperatures of the samples in my experiments. While air temperature should not vary too much over the span of

one mile, incorporating my own weather station into the experiment that sits much closer to the samples could be fruitful in improving data quality and precision.

## 4.2 Reasons for the Cooling Capacity of SEBS Polymer

The cooling capacity of the SEBS polymer could be the result of the 13 and 14 $\mu$m emissivity peaks (discussed in section 1.3 and graphed in Figure 1.3) being the dominant mode of cooling in the samples rather than the peaks around 9 $\mu$m. While the 9 $\mu$m peaks varied in magnitude depending on the sample, the 13 and 14 $\mu$m peaks were consistent for each sample, so they should impart a uniform cooling capacity to all SEBS samples (whether they contain silica beads or not). Considering the fact that the emissivity spectra in Figure 1.3 are also merely upper bounds on emissivity—rather than absolute measures of emissivity—there is a lot of room for the 9 $\mu$m peaks to be degraded from my expectations.

There may also be a heat sink in my experimental apparatus that creates an unexpected heat flow out of the samples. The styrofoam stands, while meant to be insulating, may serve as large heat sinks. This could explain the fact that even the bare aluminum plates tested in section 3.4 cooled by a degree or more. This potential heat flow could be reduced by elevating the aluminum plates slightly above the test stands. Resting on small thumb tacks instead of the bulk of the styrofoam, there should be less heat transfer between the samples and the styrofoam.

Implementing these modifications to the experimental apparatus (including more temperature measurements, including a weather station, and isolating the samples from potential heat sinks) and performing more repetitions of these experiments (so that variations can become more statistically significant in ANOVA tests) could help elucidate where the weather variations come from and determine how strong the innate cooling capacity of the SEBS polymer is. Also, performing my own FTIR measurements to get an absolute measure of sample emissivity spectra (instead of an upper bound) could help narrow down the impacts of the different emissivity peaks on cooling.

# Conclusions

In summary, my radiative cooling samples routinely accomplished single-digit cooling below the ambient air temperature. I was surprised to find that the SEBS control sample had significant cooling capabilities despite lacking an emissivity peak in the 8 to 13 $\mu$m range, implying that longer-wavelength peaks or potential heat sinks in my experimental apparatus could be sources of cooling that act uniformly across the polymer samples. I also found that weather variations play a significant role in radiative cooling capacity, although the exact relationship between weather conditions and sample cooling remains unclear. In all, further research is needed to determine whether radiative cooling can be practical in deployment conditions, as its effects are subtle and difficult to discern. My experiments demonstrated that radiative cooling is incredibly subject to weather variations, which is not what one would desire for a reliable air conditioning system. However, with further development, it could show promise in practical applications as these issues are studied and solved.

# Bibliography


[1] Zhen Chen, Linxiao Zhu, Aaswath Raman, and Shanhui Fan. Radiative cooling to deep sub-freezing temperatures through a 24-h day–night cycle. *Nature Communications*, 7, 2016. doi.org/10.1038/ncomms13729.

[2] U.S. Energy Information Administration. 2020 residential energy consumption survey (recs), table ce3.1. 2024. www.eia.gov/consumption/residential/data/2020/index.php.

[3] U.S. Energy Information Administration. 2018 commercial buildings energy consumption survey (cbecs), table e1. 2022. www.eia.gov/consumption/commercial/data/2018/index.php.

[4] National Renewable Energy Laboratory. Solar spectra. 2025. https://www2.nrel.gov/grid/solar-resource/spectra.

[5] R. Appleby and H. B. Wallace. Standoff detection of weapons and contraband in the 100 ghz to 1 thz region. *IEEE Transactions on Antennas and Propagation*, 55:2944–2956, 2007. doi.org/10.1109/TAP.2007.908543.

[6] Aaswath P. Raman, Marc Abou Anoma, Linxiao Zhu, Eden Rephaeli, and Shanhui Fan. Passive radiative cooling below ambient air temperature under direct sunlight. *Nature*, 515:540–544, 2014. doi.org/10.1038/nature13883.